PCCP

PAPER

View Article Online
View Journal | View Issue

Cite this: *Phys. Chem. Chem. Phys.*, 2021, **23**, 14391

Impact of the particle mixing state on the hygroscopicity of internally mixed sodium chloride–ammonium sulfate single droplets: a theoretical and experimental study†

Yeny A. Tobon, *[a] Danielle El Hajj,[ab] Samantha Seng,[a] Ferdaous Bengrad,[a] Myriam Moreau,[a] Nicolas Visez,[a] Isabelle Chiapello,[b] Suzanne Crumeyrolle[b] and Marie Choël *[a]

Received 10th April 2021,
Accepted 17th June 2021

DOI: 10.1039/d1cp01574e

rsc.li/pccp

Sodium chloride (NaCl) is the main constituent of sea-salt aerosols. During atmospheric transport, sea-salt aerosols can interact with gases and other particles including secondary aerosols containing ammonium sulfate ($(NH_4)_2SO_4$). This paper reports on the deliquescence relative humidity (DRH) of internally mixed sodium chloride–ammonium sulfate ($NaCl/(NH_4)_2SO_4$) coarse particles by means of an acoustic levitation system fitted with a confocal Raman microscope (CRM). The chemical composition and physical state of individual levitated particles of different initial NaCl mole fractions were monitored during the deliquescence cycle by CRM. Experimental results were compared to the data predicted by the thermodynamic model E-AIM (Extended-Aerosol Inorganics Model). We demonstrated that NH_4Cl, Na_2SO_4 and $NH_4NaSO_4{\cdot}2H_2O$ are formed in recrystallized particles and coexist with NaCl and $(NH_4)_2SO_4$. All these products are randomly distributed within the particles. Deliquescence curves described two or three-stage phase transitions depending on the initial composition of the droplet. Significant discrepancies between the model and the laboratory experiments were observed for NaCl mole fractions varying between 0.40 and 0.77 due to a divergence between the predicted and the truly present products in the particles' solid fraction during the humidification cycle.

1. Introduction

Sea-salt aerosols represent one of the most important natural aerosols in the atmosphere and are mainly composed of sodium chloride (NaCl).[1,2] During their transport in the atmosphere, particularly in areas under anthropogenic influence, sea-salt aerosols can interact with gases and other particles including secondary aerosols containing ammonium sulfate ($(NH_4)_2SO_4$), which is a predominant inorganic component of atmospheric aerosols.[3] NaCl and $(NH_4)_2SO_4$ both are hygroscopic compounds and particles containing these inorganic salts can uptake water depending on the relative humidity (RH) of the surrounding medium. Such atmospheric particles change size by water uptake or water loss and their physical–chemical properties are constantly altered. In addition, the amount of soluble and insoluble material in an aerosol particle is variable during hydration–drying processes. The constantly evolving ratio of soluble to insoluble material as a function of ambient RH is an important factor driving aerosol–cloud interactions. Soluble species are commonly found in the accumulation (0.1 μm < particle size diameter < 2.5 μm) and coarse (2.5 μm < particle size diameter < 10 μm) modes. Those species include sulfuric and nitric acids, sodium and ammonium salts, and some secondary organic species. Moreover, some soluble species such as sea-salt aerosols can also be present in particles with diameter lower than 1 μm, intimately mixed with ammonium salts.[4,5] Aerosol hygroscopicity and chemical composition were shown to play an important role in cloud droplet activation. In 2016, Väisänen *et al.*[6] estimated the hygroscopicity-dependent activation properties of aerosols and revealed that highly hygroscopic particles are more efficient in cloud droplet formation. Other authors showed that in-cloud processing increased the hygroscopicity of the aerosol particles significantly.[7–9] In addition, the study of hygroscopic properties of atmospheric aerosols is also fundamental to understand aerodynamic properties, optical properties and chemical reactivity. On the other hand, aerosols are complex and one-compound particles are far from being realistic.

[a] *Univ. Lille, CNRS, UMR 8516 - LASIRE - LAboratoire de Spectroscopie pour les Interactions, la Réactivité et l'Environnement, F-59000 Lille, France. E-mail: yeny.tobon-correa@univ-lille.fr, marie.choel@univ-lille.fr*
[b] *Univ. Lille, CNRS, UMR 8518 - LOA - Laboratoire d'Optique Atmosphérique, F-59000 Lille, France*

† Electronic supplementary information (ESI) available. See DOI: 10.1039/d1cp01574e

Therefore, consideration of multi-component aerosols is essential to understand atmospheric processes because aerosol hygroscopicity depends on the mixing state of the particles.[10,11] The solid to aqueous phase transformation is known as the deliquescence relative humidity (DRH). DRH at a given temperature refers to the water activity of a single electrolyte solution that is in equilibrium with its salt precipitate.[12] Thus, at a given temperature, solid-aqueous transition of single-component particles occurs at a characteristic RH. However, the complexity of the deliquescence transition increases with the number of hygroscopic components in the particle.[13] In addition, the distribution of chemical species within a particle can be spatially heterogeneous. This adds another level of complexity and illustrates the necessity to understand how the hygroscopic behavior of particles depends on their internal physical and chemical mixing states.[14]

Hygroscopic properties of particles containing solely NaCl or $(NH_4)_2SO_4$ are very well known.[15–23] Several authors have been interested in the hygroscopic properties of aerosols containing NaCl or $(NH_4)_2SO_4$ mixed with other inorganic salts. For example, Ge *et al.*[24] were interested in the deliquescence of NaCl/KCl, NaCl/$NaNO_3$, and $(NH_4)_2SO_4/NH_4NO_3$ mixtures. The $(NH_4)_2SO_4/NH_4NO_3$ system was very complex and experimental reports were not consistent with predictions. Nonetheless, recently, Wu *et al.*[20] achieved the study of the hygroscopic properties of the $(NH_4)_2SO_4/NH_4NO_3$ mixture and clarified the phase diagram by detection of the products by means of Raman spectroscopy. In another study, Rosenoern *et al.*[25] evidenced that the hygroscopic growth of particles initially containing $(NH_4)_2SO_4$ and H_2SO_4 was influenced by repeated RH cycles. The hygroscopic properties of mixed NaCl/$NaNO_3$ have also been studied by other authors by using optical microscopy and scanning electron microscopy coupled to energy dispersive X-ray spectroscopy (SEM/EDX),[16] and laser trapping coupled with Raman spectroscopy.[26] Similarly, Fong *et al.*[27] studied the mutual deliquescence relative humidity (MDRH) of NH_4Cl/NaCl, $NH_4Cl/(NH_4)_2SO_4$ and NaCl/NaBr mixtures. MDRH values were in agreement with those predicted by the Extended Aerosol Inorganics Model (E-AIM),[28] a program for modelling gas/liquid/solid equilibrium in chemical systems of interest to atmospheric chemistry, with the exception of the NaCl/NaBr system due to the formation of hydrated salts or complexes. On the other hand, several studies have reported the hygroscopic properties of particles containing NaCl or $(NH_4)_2SO_4$ mixed with organic compounds.[29–35]

In 1995, Potukuchi and Wexler[36] developed an equilibrium model to identify the solid-aqueous phase transformations and studied the system containing chlorine (Cl^-), sodium (Na^+), ammonium (NH_4^+) and sulfate (SO_4^{2-}) ions. The model predicted the solid composition and deliquescence transitions as a function of the mole fractions. Conversely, few works have been devoted to the experimental study of mixed NaCl/$(NH_4)_2SO_4$ particles, with only partial deliquescence reported and no possibility to determine the composition of the particle.[37,38]

In this work, DRH of internally mixed (NaCl) and ammonium sulfate ($(NH_4)_2SO_4$) coarse particles are measured using an acoustic levitation system coupled to a confocal Raman microscope (CRM). The experimental setup allows to mimic airborne particles with a droplet held in suspension using an acoustic levitator to prevent the interaction with a contacting surface and to characterize the local chemical composition during a physicochemical process. To our knowledge, this is the first laboratory study that (i) identifies the products resulting from the recombination of Na^+, Cl^-, NH_4^+ and SO_4^{2-} ions in levitated single particles with different initial compositions and (ii) directly observes their behavior during multiple deliquescence cycles. The experimentally observed phase transitions were compared to the DRH values calculated using the Extended Aerosol Inorganics Model (E-AIM).

2. Experimental methods

2.1 Sample preparation

Solid sodium chloride (NaCl, Aldrich, 99.99% purity), ammonium sulfate ($(NH_4)_2SO_4$), (Aldrich, 99.99% purity) and ultrapure deionized water (Milli-Q™, 18 MΩ) were used to prepare the 1.0 M stock solutions. Solutions with NaCl mole fractions (xNaCl) ranging from 0 to 1 were prepared by volumetric mixing of the pure NaCl and $(NH_4)_2SO_4$ stock solutions. The pH of the freshly prepared solutions was checked by pH strips.

2.2. Study of the morphology and the chemical composition of the levitated single particles

Chemical compositions of levitated single particles were studied by means of the acoustic levitation experimental setup coupled with a confocal Raman microscope (CRM) previously described in details.[39] Briefly, it consists in an ultrasonic levitator (APOS BA 10, Tec5, Germany) inside a home-made cell that allows modification of the environmental conditions (RH and T) inside the cell interfaced with a CRM for *in situ* imaging and spectral analysis of the suspended particle.

For the spectroscopic studies, we use a visible micro-Raman confocal spectrometer LabRam (Horiba Scientific, S.A.), equipped with a He–Ne laser of 633 nm (power on the sample = 6 mW), a 1800 g mm^{-1} diffraction grating, a Synapse 1024 × 256 charge-coupled device (CCD) detector, an Olympus BX40 microscope and a high-resolution video camera (Basler Ace NIR, 2048 × 2048 pixels) adapted to the optical Raman microscope.

Optical images and spectroscopic analysis of the particles were achieved by means of an Olympus 50× long working distance objective (WD 10.6 mm, N.A 0.5). The laser spot diameter is calculated around 1.5 μm and the depth of the laser focus is about 14 μm with a Δz limit around ±3 μm. Spectral resolution is calculated to be around of 3 cm^{-1}. Raman spectra were collected at room temperature (23 °C) and at variable RH ranging from 10 to 90%, in the 100–3900 cm^{-1} range with an acquisition time of 30 s for each spectrum. Relative humidity was generated and controlled by a RH Controller (Serv'instrumentation) giving a relative humidity accuracy of ±0.9%. The environmental conditions (RH and T) within the cell were verified using a SENSIRION (Model SHT85) sensor with uncertainties of ±0.1 °C and ±1.5% RH. A schematic diagram of the experimental setup is shown in Fig. S1 in the ESI.†

2.3 Investigation of the deliquescence behavior of mixed $NaCl/(NH_4)_2SO_4$ particles

The deliquescence experiments, for all solutions containing a specific NaCl mole fraction, were conducted by generating a spray of fine droplets out of a medical nebulizer (Omrom MicroAIR U22, Japan) and trapping a droplet into the acoustic field as described in previous works.[39,40] In the present study, aqueous droplets ranging from 60 to 160 μm were trapped at room temperature (23 °C) and at RH around 80%. After stabilization inside the acoustic field, droplets were dried by means of a N_2 flow until reaching a RH of 10% where particles were completely solidified and free water Raman signals were absent from the spectra. Deliquescence cycles were performed three times on fresh droplets for each fraction by slowly increasing the RH inside the cell. Changes in the 2D-projected area of the particle were monitored by optical images collected through the Raman microscope. After each deliquescence process, particles were recrystallized to compare the initial and final 2D-projected areas. The particle images were processed using ImageJ software.[41] Multicomponent aerosol surrogate particles in the coarse size range were examined for physical–chemical effects of hygroscopic ageing. Several previous works have demonstrated that DRH values of particles larger than 100 nm are not affected by initial size of the particles.[6,7,10,15,16,42,43] The growth factor (GF) of the particles during humidification was calculated from the ratio between the 2D projected area of the humidified particle (A) and the projected area of the dried particle (A_0). The uncertainties linked to the projected area measurements are about 1 pixel corresponding to 0.26 μm. The mutual deliquescence relative humidities (MDRH) and the deliquescence relative humidities (DRH) were deduced from the plots of the GF as a function of the RH (herein humidograms).

Deliquescence behaviour of several mixtures of NaCl and $(NH_4)_2SO_4$, with NaCl mole fractions varying between 0 and 1, was simulated by using the online available Extended AIM Aerosol Inorganic Model III (E-AIM-III).[44] Simulations were first performed for the RH range varying between 1.0 and 99.9%. A set of 100 points was calculated in this range, given a RH variation close to 1%. Afterwards, 100 points were again calculated in the 65 to 85% RH limited range to achieve a RH scale of 0.2%. Indeed, a finer variation of RH allows the deduction of all the deliquescence points. No limitation in the formation of solids or partitioning of trace gases was imposed. Additionally, we have combined E-AIM model results with the phase transition contours developed by Potukuchi and Wexler,[36] to anticipate the chemical composition and concentration of the species within the solid fraction of the particle. Input parameters used with E-AIM-III model are listed in Table S1 in the ESI.†

3. Results and discussion

3.1. Deliquescence relative humidity behavior of mixed $NaCl/(NH_4)_2SO_4$ particles

We investigated the deliquescent behavior of single particles prepared from 13 aqueous solutions containing different proportions of NaCl and $(NH_4)_2SO_4$: xNaCl = 0, 0.1, 0.2, 0.27, 0.36, 0.4, 0.5, 0.55, 0.6, 0.67, 0.77, 0.89 and 1. The ratios of the projected area A/A_0 obtained from the optical images were measured as a function of the relative humidity inside the chamber during humidification processes. Fig. 1 illustrates (a) the changes in the optical images of a levitated $NaCl/(NH_4)_2SO_4$ particle containing a NaCl mole fraction of 0.55 as a function of the relative humidity and (b) the deliquescence growth curve of this levitated $NaCl/(NH_4)_2SO_4$ particle. Changes in the optical images and humidograms for selected NaCl mole fractions (0.1, 0.2, 0.27, 0.36, 0.4, 0.5, 0.6, 0.67, 0.77 and 0.89) are shown in Fig. S2 in the ESI.† Table 1 summarizes the RH values of the experimental deliquescence transitions that were deduced from the humidogram curves. We have observed three deliquescence transitions identified here respectively as $MDRH_1$ (first mutual

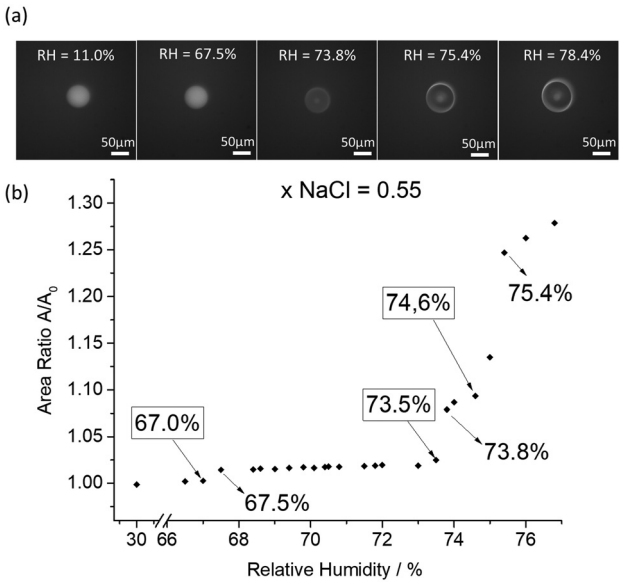

Fig. 1 (a) Optical images and (b) humidogram of a representative mixed single particle of $NaCl/(NH_4)_2SO_4$ containing a NaCl mole fraction of 0.55.

Table 1 Relative humidities corresponding to the first and second transitions ($MDRH_1$, $MDRH_2$) and to the total deliquescence (DRH) of mixed $NaCl/(NH_4)_2SO_4$ particles, ranging from 60 to 160 μm projected diameter, for different NaCl mole fractions

xNaCl	$MDRH_1$	$MDRH_2$	DRH
0	—	—	79.9 ± 0.2
0.1	69.2 ± 0.2	74.8 ± 0.3	78.4 ± 0.2
0.2	68.2 ± 0.2	74.0 ± 0.2	76.1 ± 0.3
0.27	69.0 ± 0.4	eut[a]	74.0 ± 0.3
0.36	68.3 ± 0.2	72.5 ± 0.4	75.3 ± 0.9
0.4	69.1 ± 0.2	70.5 ± 0.3	74.2 ± 0.3
0.5	67.6 ± 0.2	72.2 ± 0.2	75.2 ± 0.3
0.55	68.0 ± 0.7	73.3 ± 0.2	74.7 ± 0.2
0.6	67.5 ± 0.2	n.o	75.0 ± 0.3
0.67	68.3 ± 0.2	71.0 ± 0.2	72.3 ± 0.2
0.77	67.3 ± 0.4	n.o	73.1 ± 0.2
0.89	67.6 ± 0.4	—	73.0 ± 0.8
1	—	—	75.6 ± 0.2

[a] eut: eutonic composition.N.o: not observed experimentally.

deliquescence relative humidity), $MDRH_2$ (second mutual deliquescence relative humidity) and DRH (total deliquescence relative humidity). At the beginning of humidification, particles remain solid until reaching a typical RH where a partial deliquescence occurs. At this point, identified as $MDRH_1$, particles consist of both, a solid and an aqueous phase. The aqueous fraction consists of a saturated solution of salts, which corresponds to the *eutonic point*. A second partial deliquescence transition is observed before the total deliquescence ($MDRH_2$). At $MDRH_2$ a second fraction of the solid phase is solubilized. Hence, a second fraction of a saturated solution of salts is combined with the first saturated solution, but a solid fraction still remains into the particle. Finally, complete solubilization is achieved at a typical RH value identified as DRH, with the particle consisting only of the aqueous phase and composition is equal to the initial particle composition (see Fig. S3 in the ESI†).

Reported RH corresponds to the average value of three measurement cycles on fresh particles and the uncertainties correspond to the standard deviation of the measurements.

DRH of pure NaCl (xNaCl = 1) and pure $(NH_4)_2SO_4$ (xNaCl = 0) were first studied on single levitated particles. As expected, both compounds presented only one deliquescence transition at 75.6 ± 0.2% for pure NaCl and 79.9 ± 0.2% for pure $(NH_4)_2SO_4$, these DRH values being in agreement with those determined by previous studies.[13,16,20,45]

For the mixed NaCl/$(NH_4)_2SO_4$ particles, two or three deliquescence transitions were observed depending on the considered NaCl mole fraction. A three-stage deliquescence curve means that three or more hygroscopic compounds coexist in the particle. In binary simple mixtures, where no new compounds are formed in solid phase, deliquescence curves depict two stages ($MDRH_1$ and DRH) with exception of eutonic composition for which only one transition occurs.[26,46]

First transitions ($MDRH_1$) were not constant for all the considered fractions and varied between 67.3 and 69.2%, compatible with the observations of Cohen and coworkers (1987)[38] that measured the water activity of three fractions of NaCl/$(NH_4)_2SO_4$ mixed particles (xNaCl = 0.33, 0.50, 0.66) and determined that partial deliquescence occurred between 65 and 68%. In the first transition, which corresponds to the first mutual deliquescence relative humidity ($MDRH_1$), the aerosol consists of a solid fraction in equilibrium with an aqueous solution. Optical images did not evidence changes in the morphology of the particles. Hence, the $MDRH_1$ transitions were mainly deduced from the humidograms.

Second transitions, corresponding to the second mutual deliquescence relative humidities ($MDRH_2$), were observed to vary between 70.5 and 74.9%. As expected, the values were lower than the DRH of pure NaCl and $(NH_4)_2SO_4$. At $MDRH_2$, an additional portion of the solid particle is solubilized. The aerosol droplet consists of a smaller solid fraction than in $MDRH_1$, which was in equilibrium with a more abundant aqueous phase. An exception was confirmed for the 0.27NaCl mole fraction that corresponds to a pseudo eutonic composition, in which all the remained solid fraction is solubilized. This second transition was also not observed experimentally for the 0.6 and 0.77NaCl mole fractions, although we attributed this to the proximity of the $MDRH_1$ and $MDRH_2$ values that complicates their experimental determination. For 0.89NaCl mole fraction, only two transitions were observed, in agreement with the E-AIM model. The third transition corresponded to the total deliquescence (DRH) of the particles where the species are completely solubilized. The experimental $MDRH_1$, $MDRH_2$ and DRH for each NaCl mole fraction are reported on the phase diagram (see Fig. 7 in Section 3.3) together with values obtained by the E-AIM model. The variation of the composition of the particles during humidification will be detailed in Section 3.3.

3.2. Determination of the chemical composition of mixed single particles of NaCl/$(NH_4)_2SO_4$ during deliquescence processes

NaCl and $(NH_4)_2SO_4$ salts dissociate in water into their ions: chloride (Cl^-), sodium (Na^+), ammonium (NH_4^+) and sulfate (SO_4^{2-}). pH of the samples varies between 4.6 and 7.0. The contribution of the conjugated acid–base species, HSO_4^- and NH_3, are neglected for pH values ranging between 2.9 and 8.3 where the SO_4^{2-} and NH_4^+ species are predominant (pK_a NH_4^+/NH_3 = 9.3 at 25 °C; pK_a HSO_4^-/SO_4^{2-} = 1.9 at 25 °C). After each deliquescence cycle, particles were recrystallized and sizes of the dried particles, before and after deliquescence cycles, were compared to detect some evaporation of the products. Thus, gas phase species were neglected because sizes of the particles were unchanged during our laboratory experiments.

When a droplet containing these four ions dries up, ions are recombined forming again NaCl and $(NH_4)_2SO_4$ but also new species like NH_4Cl, Na_2SO_4 and $NH_4NaSO_4{\cdot}2H_2O$ as described in eqn (1)–(5). Thus, the deliquescence evolution of such particles results from the contribution of all these species formed after solidification. Reactions are supposed total on dehydration with formation of all the five compounds. A major quantity of NaCl or $(NH_4)_2SO_4$ is expected in NaCl or $(NH_4)_2SO_4$ rich particles, an important contribution of the other products is expected in intermediate proportions.

$$Na^+_{(aq)} + Cl^-_{(aq)} = NaCl_{(s)} \quad (1)$$

$$2NH_4^+{}_{(aq)} + SO_4^{2-}{}_{(aq)} = (NH_4)_2SO_{4(s)} \quad (2)$$

$$NH_4^+{}_{(aq)} + Cl^-_{(aq)} = NH_4Cl_{(s)} \quad (3)$$

$$2Na^+_{(aq)} + SO_4^{2-}{}_{(aq)} = Na_2SO_{4(s)} \quad (4)$$

$$NH_4^+{}_{(aq)} + Na^+_{(aq)} + SO_4^{2-}{}_{(aq)} + 2H_2O_{(l)} = NH_4NaSO_4{\cdot}2H_2O_{(s)} \quad (5)$$

In this work, the chemical composition of levitated single particles was measured on-line with CRM during humidification processes. Even if NaCl does not have Raman active vibrations, Raman spectra of the solid species $(NH_4)_2SO_4$, NH_4Cl, Na_2SO_4 and $NH_4NaSO_4{\cdot}2H_2O$ are well known and their specific vibrations make characterization unambiguous.[47–49] Fig. S4 of the ESI,† shows the Raman spectra of the pure compounds $(NH_4)_2SO_4$, NH_4Cl, Na_2SO_4 collected in our laboratory

and used as references. For $NH_4NaSO_4{\cdot}2H_2O$, we used the Raman spectra reported in previous works.[47,50,51]

The Raman spectrum of solid $(NH_4)_2SO_4$ is dominated by the sulfate symmetric stretching mode centered at 976 cm^{-1}. The other vibration modes are weak and are centered on 452, 612 and 624 cm^{-1} for the sulfate bending modes, 1065 and 1082 cm^{-1} for the sulfate antisymmetric stretching modes, 1414, 1662 and 1692 cm^{-1} for the ammonium ion bending modes, and 3129 and 3296 cm^{-1} for the ammonium ion stretching modes. Sulfate symmetric stretching mode is generally the most intense signature in sulfate containing compounds and it can be used to identify and monitor a sulfate product in a mixture.

At room temperature and atmospheric pressure, Na_2SO_4 can be formed in its crystalline forms III and V and as the hydrated form $Na_2SO_4{\cdot}10H_2O$. It is well known that at room temperature phase V is the most stable phase of Na_2SO_4. However, the metastable phase III can grow from aqueous solutions and then be transformed into phase V[52] or also be formed by crystallization of single droplets and transformed into a stable phase V during the deliquescent process.[53] Both crystalline phases have characteristic Raman signatures, mainly the symmetric stretching mode of the sulfate around 996 and 993 cm^{-1} for the phases III and V respectively.[47,54]

Regarding to $Na_2SO_4{\cdot}10H_2O$, its Raman spectrum is also well known. Its most intense and characteristic signature is the symmetric stretching mode of the sulfate around 989 cm^{-1}.[55] However, no band around 989 cm^{-1} was observed for any molar composition. In the model developed by Potukuchi and Wexler,[36] $Na_2SO_4{\cdot}10H_2O$ is predicted to be formed in systems containing high proportions of Na^+ and SO_4^{2-} ions and low proportions of Cl^- and NH_4^+ ions, which is not compatible with our experiments. Additionally, Vargas-Jentzsch and co-workers[47] observed the formation of Na_2SO_4 (III and V) and $NH_4NaSO_4{\cdot}2H_2O$ from the solid-state reactions between $(NH_4)_2SO_4$ and $Na_2CO_3{\cdot}H_2O$ at 70% RH and room temperature. No $Na_2SO_4{\cdot}10H_2O$ was evidenced. Therefore, we discarded the presence of $Na_2SO_4{\cdot}10H_2O$ in our experiments in contradiction to the hypothesis of Cohen *et al.*[38] who supposed that water remaining in the solid particle after drying would be related to the decahydrated Na_2SO_4.

Finally, the double salt $NH_4NaSO_4{\cdot}2H_2O$ was identified by the symmetric stretching mode of sulfate around 982 cm^{-1} and the O–H stretching mode of crystalline water near to 3500 cm^{-1}. NH_4Cl is mainly characterized by the sharp bands at 1402 and 1708 cm^{-1} that correspond to the bending modes of NH_4 and the N–H stretching mode at 3050 cm^{-1}.

On the other hand, in our CRM configuration, spot diameter of the focused laser beam within material is around 1.5 μm and depth of the laser focus is near to 14 μm. Levitated particles exceed these values and Raman signatures are recorded at the focal point. Therefore, detection of products depends on the local microenvironment and the arrangement of the compounds into the particle. Hence, we have performed Raman spectra from different locations on the particle surfaces. Several particles of different mole fractions were studied. Fig. 2 illustrates the heterogeneous distribution on a recrystallized single particle containing a NaCl mole fraction of 0.67. Raman bands were normalized according to the 976 cm^{-1} band. The relative intensities of the bands of the different products vary with the focal point. This result means that all compounds are randomly distributed within the particles. The quantification of each compound is highly depending on the particle orientation and the focal point. Therefore, Raman spectra are only used to detect the presence or absence of the compounds and not to quantify their concentrations.

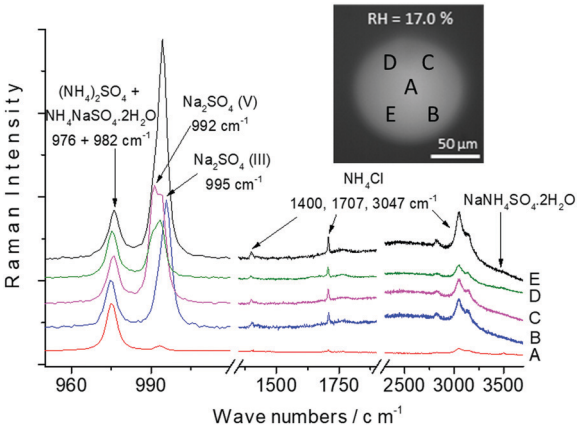

Fig. 2 Raman spectra showing the heterogeneous distribution of the products after recrystallization of a particle initially containing a mixture of NaCl/$(NH_4)_2SO_4$ (xNaCl = 0.67).

We have also used the E-AIM inorganic model to calculate the aerosol composition of the solid and the aqueous fractions during the humidification process. The model gives the molar composition by ion in the aqueous phase. Thus, remaining solid fraction is deduced from the difference between initial molar composition and the solubilized mole fraction. From the ion concentration analysis, in aqueous and in solid phases, and from the correlation between stoichiometric ratio of the ions into the species, the compounds present in each transition can be proposed. Tables S1–S4 of the ESI,† show the concentration of the ions, at different hydration levels for simulated particles initially containing 0.1, 0.36, 0.55 and 0.67NaCl mole fractions respectively. Chemical species in solid and aqueous phase and their concentration were proposed.

0.1NaCl mole fraction. Fig. 3(a) shows the Raman spectra of one representative particle upon hydration. Absence of free water in the dried particle was verified by controlling the characteristic broad Raman band of water between 3100 and 3600 cm^{-1}. Fig. 3(b) illustrates the spectral region of the sulfate symmetric stretching mode. At 21% RH, solid $(NH_4)_2SO_4$, identified by its characteristic $\nu_{as}(SO_4^{2-})$ band at 976 cm^{-1}, dominated the Raman spectra as expected. Additionally, very weak peaks around at 996 and 1706 cm^{-1}, attributed to Na_2SO_4(III) and NH_4Cl respectively, were randomly observed in different experiments on fresh particles or on the same particle after successive recrystallizations. A weak shaped band around 3500 cm^{-1} was also observed and suggested the formation of $NH_4NaSO_4{\cdot}2H_2O$ (see Fig. S5 of the ESI†). Sulfate band of this

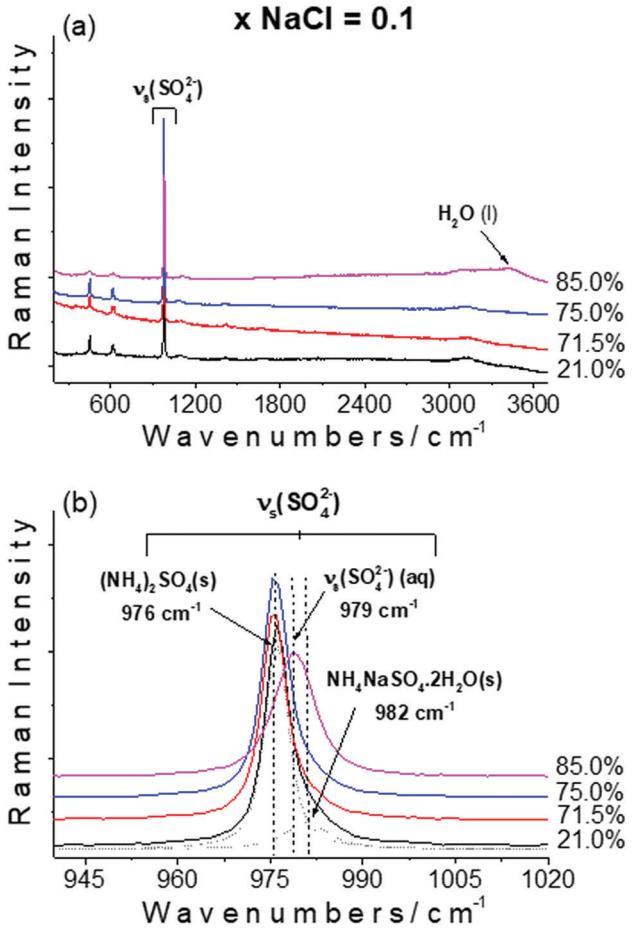

Fig. 3 Raman spectra of mixed NaCl/$(NH_4)_2SO_4$ single particles for 0.1 mole fractions of NaCl for representative RH. (a) In the 200–3700 cm^{-1} spectral range, (b) in the sulfate symmetric stretching mode region. Grey dotted lines show the deconvoluted curves from 21% RH spectrum.

double salt, expected around 982 cm^{-1}, was overlapped by the strong sulfate band of $(NH_4)_2SO_4$ and can be observed by a spectral deconvolution treatment.

To perform the E-AIM calculation, ionic composition of a 0.100 NaCl mole fraction was set to contain 1.800 mol of NH_4^+, 0.900 mol of SO_4^{2-}, 0.100 mol of Na^+ and Cl^-. Based on Potukuchi and Wexler's phase transition contours, these ionic concentrations could be interpreted as solid compound concentrations. Thus, dried particle would be composed of 0.1 mol of NH_4Cl (10.0%), 0.1 mol of $NH_4NaSO_4{\cdot}2H_2O$ (10.0%) and 0.8 mol of $(NH_4)_2SO_4$ (80.0%) as shown in Table S2 of the ESI.† Conversely, few quantities of Na_2SO_4 were evidenced in the Raman spectra. Even if it is not possible to detect NaCl in our experiments, we cannot discard its presence in the particle.

Calculated deliquescence curve predicted three deliquescence transitions ($MDRH_1$, $MDRH_2$ and DRH). The fourth ions should remain in the solid state until RH of 69.4% ($MDRH_1$), where a fraction of the solid species is solubilized. After $MDRH_1$, solid fraction composition would be reduced to 0.060 mol of Na^+, 1.570 mol of NH_4^+ and 0.815 mol of SO_4^{2-} which could fit with 0.060 mol of $NH_4NaSO_4{\cdot}2H_2O$ (7.4%) and 0.755 mol of $(NH_4)_2SO_4$ (92.6%). Subsequently, eutonic aqueous phase at $MDRH_1$ would be composed of 0.040, 0.100, 0.230 and 0.085 mol of Na^+, Cl^-, NH_4^+ and SO_4^{2-} respectively. Therefore, chloride ions were expected to solubilize completely at $MDRH_1$, while sodium, sulfate and ammonium ions were only partially solubilized. Hence, no solid species containing Cl^-, such as NaCl and NH_4Cl, should be present in the solid fraction of the particle after the first deliquescence transition. Particle Raman spectra were collected just after the first deliquescence transition ($MDRH_1$), which occurred at around 69.2 ± 0.2% (E-AIM = 69.4%). Spectra showed the absence of NH_4Cl consistently with the calculations. We assumed that if some NaCl was initially present in the solid particle, it was also completely dissolved at $MDRH_1$ in agreement with calculations where no solid chlorine species is expected after the first transition. A small quantity of $NH_4NaSO_4{\cdot}2H_2O$ was expected to remain in the solid fraction after $MDRH_1$, however, we did not evidence its characteristic Raman features on the spectra. Raman signatures could be covered by the noise. Thus, only $(NH_4)_2SO_4$ and Na_2SO_4 were clearly evidenced in the solid fraction. The aqueous fraction was then formed by solubilization of NaCl, NH_4Cl, $NH_4NaSO_4{\cdot}2H_2O$ and some quantity of $(NH_4)_2SO_4$. Characteristic broad Raman band of water around 3400 cm^{-1} was not evidenced at $MDRH_1$ as would expected after solubilization of a fraction of the solid particle. Furthermore, as water has a weak Raman signal, a very thin film of water on the particle surface could explain its absence from the spectrum.

Second deliquescence transition was predicted to occur at 73.8% and observed experimentally at about 74.8 ± 0.3%. After $MDRH_2$, solid fraction would be composed of 1.26 mol of NH_4^+ and 0.630 mol of SO_4^{2-}, which is consistent with a single component, the $(NH_4)_2SO_4$ (0.630 mol). Accordingly, 0.125 mol of $(NH_4)_2SO_4$ and 0.060 mol of $NH_4NaSO_4{\cdot}2H_2O$ would dissolve at $MDRH_2$. Raman studies confirmed the presence of only $(NH_4)_2SO_4$ in the solid fraction after the second deliquescence transition. Therefore, no Na-containing species was detected in the solid particle after the $MDRH_2$ in agreement with the E-AIM model.

As predicted, complete deliquescence (DRH) occurred at around 78.4 ± 0.2%. Raman spectra showed only the signatures of aqueous NH_4^+ and SO_4^{2-} ions. In addition, OH stretching vibration modes of free water (broadband near to 3400 cm^{-1}) were observed to increase in the Raman spectra, as expected for an aqueous droplet. Table 2 summarizes the solid chemical species observed during humidification process.

0.36NaCl mole fraction. Raman spectra as a function of RH obtained for one of the trapped particles are presented in Fig. 4(a). The spectral region of the sulfate symmetric stretching mode is presented in Fig. 4(b). One can note the absence of free water on the dried solid particles. $(NH_4)_2SO_4$, NH_4Cl, Na_2SO_4(III) and $NH_4NaSO_4{\cdot}2H_2O$ were evidenced by their characteristic Raman signatures. As expected, formation of the new species by combination of Na^+ and Cl^- ions with NH_4^+ and SO_4^{2-} ions seemed to increase. Ionic composition of the dried solid particle deduced from E-AIM model was interpreted by using Potukuchi and Wexler's phase transition contour. It is expected to be composed of 0.280 mol of $(NH_4)_2SO_4$ (28.0%), 0.360 mol of

Table 2 Chemical species in single particles prepared by mixing NaCl and $(NH_4)_2SO_4$ (xNaCl = 0.1, 0.36, 0.55 and 0.67). Solid species in particles before and after deliquescence transitions ($MDRH_1$ and $MDRH_2$). Comparison between solid species observed by Raman spectroscopy (main Raman bands are indicated in parentheses) and deduced from E-AIM model

	Dried particle		$MDRH_1$		$MDRH_2$	
x(NaCl) = 0.1	E-AIM (%)	Raman	E-AIM (%)	Raman	E-AIM (%)	Raman
$(NH_4)_2SO_4$	80.0	Detected (976 cm^{-1})	92.6	Detected (976 cm^{-1})	100.0	Detected (976 cm^{-1})
NH_4Cl	10.0	Detected (1706 cm^{-1})	0.0	—	0.0	—
$NH_4NaSO_4{\cdot}H_2O$	10.0	Detected[a] (3500 cm^{-1})	7.4	—	0.0	—
Na_2SO_4	0.0	Detected[a] (996 cm^{-1})	0.0	Detected[a] (996 cm^{-1})	0.0	—
NaCl	0.0	NRA	0.0	NRA	0.0	NRA
x(NaCl) = 0.36						
$(NH_4)_2SO_4$	28.0	Detected (976 cm^{-1})	35.1	Detected (976 cm^{-1})	0.0	Detected (976 cm^{-1})
NH_4Cl	36.0	Detected (1706 cm^{-1})	0.0	Detected (1706 cm^{-1})	0.0	Detected (1706 cm^{-1})
$NH_4NaSO_4{\cdot}H_2O$	36.0	Detected (3500 cm^{-1})	64.9	Detected (3500 cm^{-1})	100.0	Detected (3500 cm^{-1})
Na_2SO_4	0.0	Detected (996 cm^{-1})	0.0	Detected (996 cm^{-1})	0.0	—
NaCl	0.0	NRA	0.0	NRA	0.0	NRA
x(NaCl) = 0.55						
$(NH_4)_2SO_4$	0.0	Detected (976 cm^{-1})	0.0	Detected (976 cm^{-1})	0.0	—
NH_4Cl	45.0	Detected (1706 cm^{-1})	44.5	Detected (1706 cm^{-1})	0.0	Detected (1706 cm^{-1})
$NH_4NaSO_4{\cdot}H_2O$	45.0	Detected (3500 cm^{-1})	55.5	Detected (3500 cm^{-1})	100.0	Detected (3500 cm^{-1})
Na_2SO_4	0.0	Detected (996 cm^{-1})	0.0	Detected (996, 992 cm^{-1})	0.0	—
NaCl	10.0	NRA	0.0	NRA	0.0	NRA
x(NaCl) = 0.67						
$(NH_4)_2SO_4$	0.0	Detected (976 cm^{-1})	0.0	Detected (976 cm^{-1})	0.0	—
NH_4Cl	56.0	Detected (1706 cm^{-1})	57.3	Detected (1706 cm^{-1})	0.0	Detected (1706 cm^{-1})
$NH_4NaSO_4{\cdot}H_2O$	9.5	Detected (3500 cm^{-1})	9.3	—	60.8	—
Na_2SO_4	23.5	Detected (996, 992 cm^{-1})	24.4	Detected (992 cm^{-1})	39.2	Detected (992 cm^{-1})
NaCl	11.0	NRA	9.3	NRA	0.0	NRA

[a] Few quantities.NRA: non-Raman active.

NH_4Cl (36.0%) and 0.360 mol of $NH_4NaSO_4{\cdot}2H_2O$ (36.0%) as described in Table S3 of the ESI.† All these compounds were evidenced experimentally in the solid particles by their Raman spectra before increasing RH inside the levitation cell. Nonetheless, Na_2SO_4 was also detected experimentally by its Raman signatures. Also, we do not dismiss the presence of some quantities of NaCl, even if it is not possible to confirm by Raman spectroscopy.

E-AIM simulation on 0.36NaCl mole fraction revealed a three-stage deliquescence behavior: $MDRH_1$, $MDRH_2$ and DRH. $MDRH_1$ was observed at 68.3 ± 0.2% (E-AIM = 69.4%). E-AIM model anticipates that all Cl^- ions should dissolve at that point with only 0.117 mol of $(NH_4)_2SO_4$ (35.1%) and 0.216 mol of $NH_4NaSO_4{\cdot}2H_2O$ (64.9%) remaining in solid phase. Thus, all the NH_4Cl should be completely dissolved, together with part of $(NH_4)_2SO_4$, and $NH_4NaSO_4{\cdot}2H_2O$. Consequently, the aqueous fraction (eutonic composition) should have the same ionic composition than the 0.1NaCl mole fraction (0.144 mol of Na^+, 0.360 mol of Cl^-, 0.830 mol of NH_4^+ and 0.307 mol of SO_4^{2-}). Nonetheless, all the products, except NaCl, were experimentally detected within the solid fraction after the first deliquescent point using the Raman spectra. This inconsistency confirms the complexity of the mixture and one could suppose some gaps in the model. Experimental evidences suggest that aqueous phase at $MDRH_1$ was produced by solubilization of some $(NH_4)_2SO_4$, a few quantity of NH_4Cl. Again, one could assume that all NaCl was solubilized. Characteristic broad Raman band of water around 3400 cm^{-1} was not evidenced at $MDRH_1$. Liquid Water might be present on aerosol surfaces but in such low quantities that Raman spectra was unable to detect it.

$MDRH_2$, initially expected around 71.5% (E-AIM), occurred near to 72.5 ± 0.4%. $(NH_4)_2SO_4$, NH_4Cl and $NH_4NaSO_4{\cdot}2H_2O$ were identified in the solid fraction by their characteristic Raman signatures. On the contrary, E-AIM model predicted no-chloride products within solid particle where only $NH_4NaSO_4{\cdot}2H_2O$ would remain. In addition, intensities of solid $(NH_4)_2SO_4$ and NH_4Cl decreased in comparison to intensities observed at $MDRH_1$. Therefore, aqueous fraction is produced after solubilization of Na_2SO_4 and some quantities of $(NH_4)_2SO_4$ and NH_4Cl.

Total deliquescence occurred experimentally at 75.3 ± 0.9% (E-AIM = 75.6%). Only the signatures of aqueous NH_4^+ and SO_4^{2-} ions in addition to liquid water signature were observed in the Raman spectra. No characteristic Raman signal from solid species was detected. Table 2 summarizes the solid chemical species observed during humidification process.

0.55NaCl mole fraction. Dried solid particles were monitored by Raman and liquid water signature was not evidenced (see Fig. 5). Taking into account the E-AIM model and the Potukuchi and Wexler's phase transition contour, initial dried solid particle would be composed of 0.100 mol of NaCl (10.0%), 0.450 mol of NH_4Cl (45.0%), and 0.450 mol of $NH_4NaSO_4{\cdot}2H_2O$ (45.0%) as presented in Table S4 of the ESI.† However, not only NH_4Cl and $NH_4NaSO_4{\cdot}2H_2O$ but also $(NH_4)_2SO_4$ and Na_2SO_4(III) were evidenced into the solid particle by their characteristic Raman signatures. NaCl was also presumed to coexist with

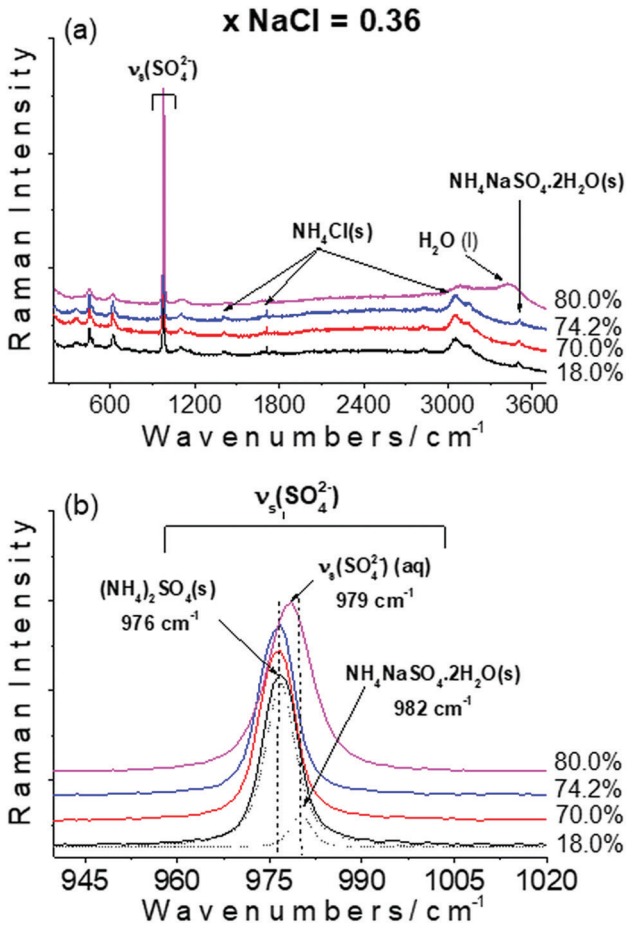

Fig. 4 Raman spectra of mixed NaCl/$(NH_4)_2SO_4$ single particles for 0.36 mole fractions of NaCl for representative RH. (a) In the 200–3700 cm^{-1} spectral range, (b) in the sulfate symmetric stretching mode region. Grey dotted lines show the deconvoluted curves from 18% RH spectrum.

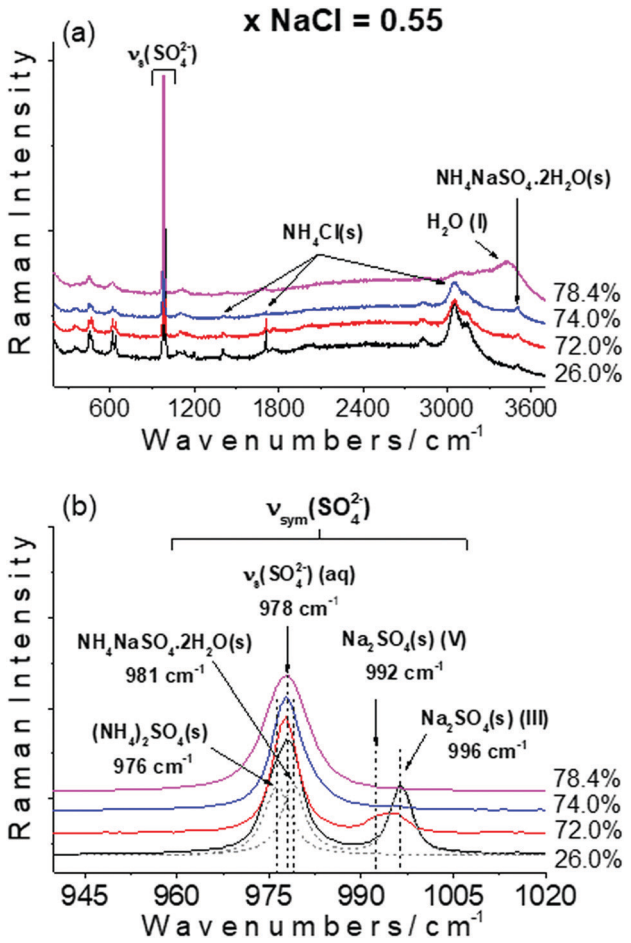

Fig. 5 Raman spectra of mixed NaCl/$(NH_4)_2SO_4$ single particles for 0.55 mole fractions of NaCl for representative RH. (a) In the 200–3700 cm^{-1} spectral range, (b) in the sulfate symmetric stretching mode region. Grey dotted lines show the deconvoluted curves from 26% RH spectrum.

these salts. Raman spectra showed a relative increase in the intensities of the characteristic Raman signatures of NH_4Cl, Na_2SO_4 and $NH_4NaSO_4{\cdot}2H_2O$. Fig. 5(a) shows the Raman spectra, when increasing RH, obtained for one of the studied particles containing 0.55NaCl mole fraction. The spectral region of the sulfate symmetric stretching mode is presented in Fig. 5(b).

The first transition occurred about 68.0 ± 0.7% (E-AIM = 68.4%) and Raman spectra showed that all the compounds, initially detected in the dried particle, remained in the solid fraction and only a slight decrease of NH_4Cl and $(NH_4)_2SO_4$ Raman band intensities was observed. In addition, a new Raman band, around 992 cm^{-1}, appeared in the spectra and was identified as the orthorhombic phase V of crystalline Na_2SO_4. This transformation was already documented as a result of the increase in RH during hydration cycle.[53] Characteristic broad Raman band of water around 3400 cm^{-1} was not evidenced at $MDRH_1$. E-AIM model, to the contrary, predicted a solid fraction composed of 0.385 mol of Na^+, 0.309 mol of Cl^-, 0.694 mol of NH_4^+ and 0.385 mol of SO_4^{2-} that fit with 0.309 mol of NH_4Cl (44.5%) and 0.385 mol of $NH_4NaSO_4{\cdot}2H_2O$ (55.5%) after $MDRH_1$.

RH in the cell reach $MDRH_2$ around 73.3 ± 0.2%. According to E-AIM model, $MDRH_2$ was expected around 70.2% and only $NH_4NaSO_4{\cdot}2H_2O$ would remain in the solid phase. In fact, after $MDRH_2$, Raman Spectra revealed the presence of NH_4Cl in addition to $NH_4NaSO_4{\cdot}2H_2O$ in the solid phase. Consequently, the discrepancy between experimental and calculated $MDRH_2$ values could be explained by the difference in the solid species truly present in the particle after $MDRH_1$ and those predicted by the model.

Finally, when RH reached 74.7 ± 0.2% the particle was completely deliquesced (DRH). This value was slightly lower than the value predicted by E-AIM (75.8%). Only the bands corresponding to aqueous species were detected in Raman spectra. In addition, optical images showed a completely transparent droplet. Table 2 summarizes the solid chemical species observed during humidification process.

0.67NaCl mole fraction. Raman spectra as a function of RH obtained for one of the trapped particles are presented in Fig. 6(a). The spectral region of the sulfate symmetric stretching mode is presented in Fig. 6(b). Raman spectra on dried solid particles did not show liquid water. According to the E-AIM

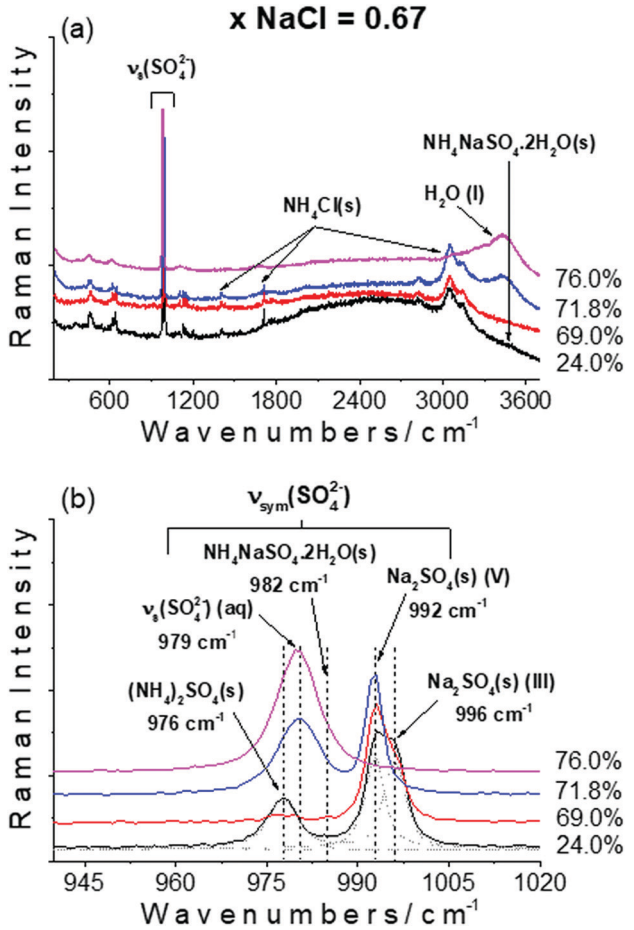

Fig. 6 Raman spectra of mixed NaCl/$(NH_4)_2SO_4$ single particles for 0.67 mole fractions of NaCl for representative RH. (a) In the 200–3700 cm^{-1} spectral range, (b) in the sulfate symmetric stretching mode region. Grey dotted lines show the deconvoluted curves from 24% RH spectrum.

model and the Potukuchi and Wexler's phase transition contour, the initial dried solid particles are expected to contain 0.110 mol of NaCl (11.0%), 0.560 mol of NH_4Cl (56.0%), 0.235 mol of Na_2SO_4 (23.5%) and 0.095 mol of $NH_4NaSO_4{\cdot}2H_2O$ (9.5%) as shown in Table S5 in the ESI.† No $(NH_4)_2SO_4$ is expected to remain in dried particle. However, solid $(NH_4)_2SO_4$, NH_4Cl, Na_2SO_4 (III and V) and $NH_4NaSO_4{\cdot}2H_2O$ were evidenced by their characteristic Raman signatures. Likewise, some NaCl remaining in solid phase is not discarded but cannot be observed in the Raman spectra during the humidification process.

The first deliquescence transition ($MDRH_1$) was observed at 68.3 ± 0.2% (E-AIM = 67.7%). Raman spectra evidenced that $(NH_4)_2SO_4$(s) and NH_4Cl(s) Raman intensities decreased and Na_2SO_4(III) was converted into Na_2SO_4(V). In contrast, characteristic Raman signature of solid $NH_4NaSO_4{\cdot}2H_2O$ disappeared from the spectrum. Thus, we assume that aqueous fraction was obtained by solubilization of $NH_4NaSO_4{\cdot}2H_2O$, NaCl and few quantities of $(NH_4)_2SO_4$ and NH_4Cl. Consequently, after $MDRH_1$, a quantity of $(NH_4)_2SO_4$, NH_4Cl and Na_2SO_4 remained in solid state. Characteristic broad Raman band of water around 3400 cm^{-1} was not evidenced at $MDRH_1$.

In contrast, E-AIM model predicted a solid phase composed of 9.3% of $NH_4NaSO_4{\cdot}2H_2O$ (0.090 mol) together with 9.3% of NaCl (0.090 mol), 57.3% of NH_4Cl (0.550 mol) and 24.4% of Na_2SO_4 (0.235 mol). Indeed, the aqueous phase is predicted to be composed of 0.020 mol of Na^+, 0.030 mol of Cl^-, 0.020 mol of NH_4^+ and 0.005 mol of SO_4^{2-}, which was interpreted as the solubilization of 0.020 mol of NaCl, 0.010 mol of NH_4Cl and 0.005 mol of $NH_4NaSO_4{\cdot}2H_2O$.

A second deliquescence transition ($MDRH_2$) was observed around 71.0 ± 0.2%, far from the RH predicted by the E-AIM model (68.4%). Raman spectra of the particles indicated the presence of NH_4Cl and Na_2SO_4(v) in solid state. The relative intensities of the Raman bands of NH_4Cl decreased, but its presence in the solid phase after the $MDRH_2$ is irrefutable. Additionally, solid $(NH_4)_2SO_4$ disappeared completely or the intensity of its sulfate symmetric stretching vibration (its most intense band) was very low and hidden by the noise. Consequently, aqueous phase was formed by solubilization of $(NH_4)_2SO_4$ and part of NH_4Cl. As mentioned, E-AIM predicted a RH value very different from the value found experimentally. In fact, E-AIM model predicted that no chlorine containing compounds remained in solid phase after the second DRH transition, and that the solid fraction would be composed of 0.207 mol of Na^+, 0.090 mol of NH_4^+ and 0.148 mol of SO_4^{2-}, interpreted as 0.090 mol of $NH_4NaSO_4{\cdot}2H_2O$ (60.8%) and 0.058 mol of Na_2SO_4 (39.2%) as described in Table S5 of the ESI.† However, contrary to the predictions, we observed that $NH_4NaSO_4{\cdot}2H_2O$ was solubilized in the first DRH transition and NH_4Cl was still present after $MDRH_2$, which could explain the clear disagreement with the model.

Finally, total deliquescence (DRH) was observed around 72.3 ± 0.2% of RH (E-AIM = 73.0%). Only the bands corresponding to aqueous species were detected in Raman spectra. In addition, optical images showed completely transparent droplets. Table 2 summarizes the solid chemical species observed during humidification process.

3.3. Deliquescence phase diagram of mixed NaCl/($(NH_4)_2SO_4$) particles

Fig. 7 shows the $MDRH_1$, $MDRH_2$ and DRH values obtained experimentally in levitation experiments for 13 mixtures of NaCl and ($(NH_4)_2SO_4$) as a function of the NaCl mole fraction. DRH values, obtained by E-AIM model for several proportions of NaCl and $(NH_4)_2SO_4$ are also reported in Fig. 7. The simulated diagrams describe two or three transitions, depending on the NaCl mole fraction. Experimental data are observed to follow moderately the transition patterns for $(NH_3)_2SO_4$ (xNaCl < 0.28) and NaCl rich particles (xNaCl > 0.87).

$MDRH_1$, corresponding to eutonic mixture, is not predicted to be constant for all mixtures and takes three values depending on the NaCl mole fractions: 69.4% from 0.01 to 0.49, 68.5% from 0.50 to 0.66 and 67.7% from 0.67 to 0.99. The experimental $MDRH_1$ values also tend to be slightly lower than predicted and decrease with xNaCl. A lower $MDRH_1$ value could suggest that particles are slightly more hygroscopic than expected. Thermodynamically, in a system containing two salts, the MDRH remains constant.

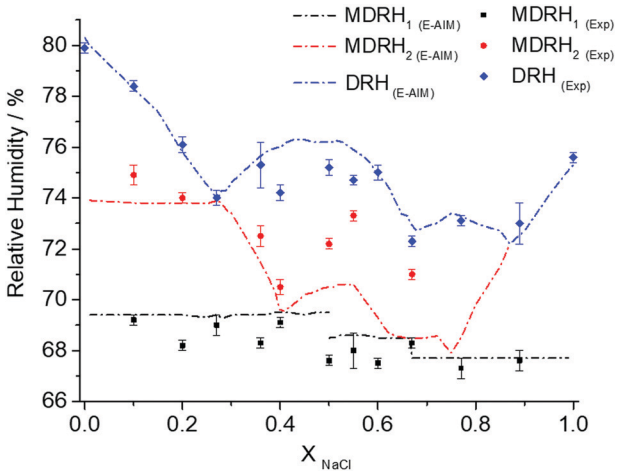

Fig. 7 Deliquescence phase diagram of mixed NaCl/$(NH_4)_2SO_4$ particles as a function of the NaCl mole fraction. Comparison of the E-AIM model results (dashed lines) with our experimental data (scatter). $MDRH_1$ (black) and $MDRH_2$ (red) refers to the first and second transitions before the total deliquescence, DRH (blue).

It is independent of the mixing ratio because water activity governs the phase transition of mixed salts at the eutonic point.[16,46] Consequently, variability in the $MDRH_1$ values found by E-AIM model is explained by the absence of one or more species in the initial solid particle as described in Tables S1–S4 of the ESI.† In our results, $MDRH_1$ behavior is irregular and fluctuated between 69.2 and 67.3%. For the four studied mixtures, Raman spectra evidence the coexistence of $(NH_4)_2SO_4$, NH_4Cl, Na_2SO_4 and $NH_4NaSO_4{\cdot}2H_2O$. We cannot discard that some NaCl is also present in the crystallized particle. However, if all the products are present in the dried particles, $MDRH_1$ value should remain constant in our experiments for all the fractions because only variable mixing ratio is expected. This contradiction could be due to the physical and chemical heterogeneity and the internal mixing state of the products within the particles. In consequence, water uptake and other properties are variable and non-uniform due to a complex chemical mixing state in the single particles. In addition, as suggested by Rosenoern *et al.*[25] the presence of a nanocrystalline morphology would also modify the particle hygroscopic behaviour. Thus, we hypothesize that aqueous solution formed at $MDRH_1$ would result from a contribution of a number of local microenvironments as a consequence of the complex internal mixing state and structural heterogeneities at the single particle scale.

Experimental $MDRH_2$ transitions are in relatively good agreement with modeled curve for xNaCl values lower than 0.4. In a binary system, the second deliquescence transition (total deliquescence) depends only on the solid salt still present after the first transition. However, in a more complex system, other deliquescence transitions can be observed before the total deliquescence. In our case, a second deliquescence relative humidity was observed for several compositions. Nonetheless, its trend appears to be continuous when xNaCl is lower than 0.27 and becomes irregular for higher fractions. E-AIM model predicts that $MDRH_2$ remains constant at 73.8% for NaCl mole fraction lower than 0.28 and then decreases gradually between 0.29 and 0.40NaCl mole fraction until reaching 69.5%. Between 0.41 and 0.75NaCl mole fraction, modeled $MDRH_2$ shows a discrete evolution first increasing until reaching a RH of 70.6% for xNaCl = 0.55 and then decreasing until reaching a RH of 67.9% for xNaCl $>$ 0.7. Experimental results are in agreement with the pattern of the model and show a maximum RH value at xNaCl = 0.55. Nevertheless, experimental $MDRH_2$ values are observed higher than predicted ones. Such a disagreement can be explained by the difference between the products predicted to remain in solid fraction after $MDRH_2$ and these truly present in the levitated particle, as for example NH_4Cl that should have been solubilized at $MDRH_2$ but was detected in the solid fraction after this transition. Finally, $MDRH_2$ is expected to increase gradually from xNaCl = 0.75 until combination with the DRH curve for the 0.87 mole fraction. No $MDRH_2$ transition was observed experimentally for xNaCl = 0.77. However, $MDRH_2$ seems to occur very close to $MDRH_1$ with a difference of only 0.8% RH according to E-AIM predictions. Thus, both transitions could be overlapped.

Concerning the DRH curve, the model reproduces very well the experimental values for $(NH_4)_2SO_4$ rich particles (xNaCl $<$ 0.36) and NaCl rich particles (xNaCl $>$ 0.77). Simulated DRH started at 80.3%, as expected for pure $(NH_3)_2SO_4$, and then DRH decreased progressively until reaching 74.3% (xNaCl $\leq$ 0.28). For NaCl mole fractions greater than 0.87, the predicted DRH values increase progressively until reaching 75.3%, in agreement with the simulated DRH value of pure NaCl. For particle chemical compositions ranging from 0.28 to 0.87NaCl mole fractions, the modeled curve is characterized by an irregular pattern describing a maximum RH value of 76.3%. Experimental DRH values were observed lower than those obtained by the model for compositions ranging from 0.40 to 0.67NaCl mole fractions, probably due to the products present in the solid phase.

The simulated diagram also shows some specific mole fractions (0.27, 0.40 and 0.87) that resemble eutonic points of complex mixtures where two transitions merged into one and only two transitions occur. Experimentally, we studied 0.27 and 0.40NaCl mole fractions. However, only 0.27NaCl mole fraction presents two transitions corresponding to $MDRH_1$ and DRH (69.0 $\pm$ 0.4% and 74.0 $\pm$ 0.3% respectively). For 0.40NaCl mole fraction, we observe three transitions in disagreement with the model ($MDRH_1$ = 69.1 $\pm$ 0.2%, $MDRH_2$ = 70.5 $\pm$ 0.3%, DRH = 74.2 $\pm$ 0.3%). In contrast, we observe only two transitions for the 0.60 and 0.77NaCl mole fractions ($MDRH_1$ and $MDRH_2$ expected to be too close), in disagreement with the model that predicted three transitions. In this case, experimentally both transitions could not be distinguished with our setup ($MDRH_1$ = 67.3 $\pm$ 0.4%, $MDRH_2$ = not observed, DRH = 73.1 $\pm$ 0.2%). We suppose that the difference between $MDRH_1$ and $MDRH_2$ would be lower than RH accuracy of the RH controller ($\pm$0.9%). Even if E-AIM simulation predicts that $MDRH_1$ and $MDRH_2$ values are also expected to be very close for the 0.60NaCl mole fraction ($MDRH_1$ = 68.5%, $MDRH_2$ = 69.3%),

the trend of the experimental data could suppose that $MDRH_2$ would be closer to DRH ($75.0 \pm 0.3\%$) than $MDRH_1$. However, it was not possible to observe this transition in our experiments. Thus, our results do not allow to evaluate if this hypothetical transition occurs too close to the first or the last transition point or if it does not occur at all.

4. Conclusions

Sea-salt aerosols represent one of the largest natural aerosol species present in the atmosphere, with sodium chloride (NaCl) as their main constituent. During their transport in the atmosphere, sea salt aerosols can interact with gases and other particles including secondary organic aerosols containing ammonium sulfate ($(NH_4)_2SO_4$). We have studied the deliquescence relative humidity of internally mixed NaCl and ammonium sulfate ($(NH_4)_2SO_4$) on coarse particles by means of an acoustic levitation system to mimic airborne particles and prevent the interaction with a contacting surface. To our knowledge, this is the first experimental work to observe and characterize the products resulting from the recombination of Na^+, Cl^-, NH_4^+ and SO_4^{2-} on levitated single particles with different initial compositions and to study their behavior during deliquescence cycles.

Deliquescence behavior of individual particles with variable initial composition was studied by optical microscopy and chemical composition was followed by confocal Raman microscopy (CRM). Additionally, experimental results were compared with those obtained with the thermodynamic model E-AIM (Extended Aerosol Inorganic Model) and the Potukuchi and Wexler's phase transition contour. Solid single particles obtained after drying levitated droplets, containing initially different proportions of the two titled compounds, showed a complex mixing state as a function of RH. Thus, we have confirmed, by means of Raman spectra, the coexistence of four solid salts within the dry particle: $(NH_4)_2SO_4$, NH_4Cl, Na_2SO_4 and $NH_4NaSO_4{\cdot}2H_2O$. As NaCl is not active in Raman, we assumed that NaCl was also present in the recrystallized droplets. Accordingly, samples are better described as multiphasic systems than as a binary system. Particles containing 0.1, 0.36, 0.55 and 0.67NaCl mole fractions were studied by CRM during the deliquescence process. Raman spectra evidenced unambiguously the presence of solid compounds that were not anticipated by the E-AIM model and the Potukuchi and Wexler's phase transition contour after each transition.

Deliquescence phase diagram was built experimentally by performing multiple deliquescence cycles of numerous mixtures with composition varying between 0.0 and 1.0NaCl mole fractions. Humidograms showed two or three transitions depending on the initial molar composition which is representative for complex systems. Experimental phase diagram showed several differences with the one built from the E-AIM model. For NaCl rich particles (xNaCl > 0.77) and $(NH_4)_2SO_4$ rich particles (xNaCl < 0.40) description made by the model is acceptable. However, for intermediate mixtures ($0.40 < x$NaCl < 0.77), experimental results disagree with the model due to a difference between predicted products remained in solid state after the transitions and the products truly present in the solid particle. Thus, our results show the difficulty of accurate modeling of humidification processes when the complexity of the aerosol chemical composition increases.

The study of the hygroscopicity and the chemical composition of complex aerosols in laboratory, without the influence of a contacting surface, is essential to understand the physicochemical processes of the aerosols during their transport in the atmosphere and their consequences on clouds and climate. A complex interplay between initial particle mixing state and variable RH was shown to greatly influence compositional and structural evolution of particles during atmospheric ageing. The results presented in this work are of importance in atmospheric chemistry because they contribute to a better understanding of the complex physicochemical changes of real aged sea-salts aerosols. Furthermore, current experimental methods available to link the diversity of particle chemistry and physical phase state to differences in the hygroscopic behavior of aerosols are relatively scarce. Owing to findings of such experimental work, aerosol thermodynamics models could be improved to produce more refined data about water uptake, phase transitions and the ability of individual particles to grow into cloud droplets as a function of the mixing state.

Author contributions

Conceptualization, M. C., S. C. and Y. T.; data curation Y. T., D. E.-H., M. C., formal analysis, Y. A. T., D. E.-H, F. B., S. S., M. C., S. C.; funding acquisition, M. C, S. C., I. C., N. V.; investigation, D. E.-H., F. B, S. S., Y. A. T., M. C., S. C.; methodology, Y. A. T., M. C, S. C.; project administration, M. C., S. C., I. C.; resources, M. C. M. M.; supervision, M. C., S. C. I. C.; validation, Y. A. T., M. C, S. C.; visualization, Y. A. T., M. C., S. C.; writing – original draft, Y. A. T.; writing – review & editing, M. C., S. C., I. C., N. V., Y. A. T.

Conflicts of interest

There are no conflicts of interest to declare.

Acknowledgements

This work was supported by funds from Labex CaPPA WP-2 and the CPER research project CLIMIBIO. The CaPPA project (Chemical and Physical Properties of the Atmosphere) is funded by the French National Research Agency (ANR) through the PIA (Programme d'Investissement d'Avenir) under contract ''ANR-11-LABX-0005-01''. The authors thank the French Ministère de l'Enseignement Supérieur et de la Recherche, the Hauts-de-France Region and the European Funds for Regional Economic Development for their financial support to this project. M. C., N. V. and S. C. thanks the Université de Lille and the Institut de Recherches Pluridisciplinaires en

Sciences de l'Environnement (IREPSE Fed 4129) for financial support.

Notes and references

1 H. Liao, W.-T. Chen and J. H. Seinfeld, Role of climate change in global predictions of future tropospheric ozone and aerosols, *J. Geophys. Res. Atmospheres*, 2006, **111**, D12304.
2 D. M. Murphy, K. D. Froyd, H. Bian, C. A. Brock, J. E. Dibb, J. P. DiGangi, G. Diskin, M. Dollner, A. Kupc, E. M. Scheuer, G. P. Schill, B. Weinzierl, C. J. Williamson and P. Yu, The distribution of sea-salt aerosol in the global troposphere, *Atmos. Chem. Phys.*, 2019, **19**, 4093–4104.
3 B. H. Baek and V. P. Aneja, Measurement and Analysis of the Relationship between Ammonia, Acid Gases, and Fine Particles in Eastern North Carolina, *J. Air Waste Manage. Assoc.*, 2004, **54**, 623–633.
4 R. M. Kirpes, A. L. Bondy, D. Bonanno, R. C. Moffet, B. Wang, A. Laskin, A. P. Ault and K. A. Pratt, Secondary sulfate is internally mixed with sea spray aerosol and organic aerosol in the winter Arctic, *Atmos. Chem. Phys.*, 2018, **18**, 3937–3949.
5 T. S. Bates, V. N. Kapustin, P. K. Quinn, D. S. Covert, D. J. Coffman, C. Mari, P. A. Durkee, W. J. D. Bruyn and E. S. Saltzman, Processes controlling the distribution of aerosol particles in the lower marine boundary layer during the First Aerosol Characterization Experiment (ACE 1), *J. Geophys. Res.: Atmos.*, 1998, **103**, 16369–16383.
6 O. Väisänen, A. Ruuskanen, A. Ylisirniö, P. Miettinen, H. Portin, L. Hao, A. Leskinen, M. Komppula, S. Romakkaniemi, K. E. J. Lehtinen and A. Virtanen, In-cloud measurements highlight the role of aerosol hygroscopicity in clouddroplet formation, *Atmos. Chem. Phys.*, 2016, **16**, 10385–10398.
7 Z. Levin, E. Ganor and V. Gladstein, The effects of desert particles coated with sulfate on rain formation in the eastern Mediterranean, *J. Appl. Meteorol.*, 1996, **35**, 1511–1523.
8 S. Crumeyrolle, L. Gomes, P. Tulet, A. Matsuki, A. Schwarzenboeck and K. Crahan, Increase of the aerosol hygroscopicity by cloud processing in a mesoscale convective system: a case study from the AMMA campaign, *Atmos. Chem. Phys.*, 2008, **8**, 6907–6924.
9 S. Henning, K. Dieckmann, K. Ignatius, M. Schäfer, P. Zedler, E. Harris, B. Sinha, D. van Pinxteren, S. Mertes, W. Birmili, M. Merkel, Z. Wu, A. Wiedensohler, H. Wex, H. Herrmann and F. Stratmann, Influence of cloud processing on CCN activation behaviour in the Thuringian Forest, Germany during HCCT-2010, *Atmos. Chem. Phys.*, 2014, **14**, 7859–7868.
10 C. N. Cruz and S. N. Pandis, Deliquescence and Hygroscopic Growth of Mixed Inorganic–Organic Atmospheric Aerosol, *Environ. Sci. Technol.*, 2000, **34**, 4313–4319.
11 X. Wang, X. Ye, J. Chen, X. Wang, X. Yang, T.-M. Fu, L. Zhu and C. Liu, Direct links between hygroscopicity and mixing state of ambient aerosols: estimating particle hygroscopicity from their single-particle mass spectra, *Atmos. Chem. Phys.*, 2020, **20**, 6273–6290.
12 A. S. Wexler and J. H. Seinfeld, Second-generation inorganic aerosol model, *Atmos. Environ., Part A*, 1991, **25**, 2731–2748.
13 S. T. Martin and Phase Transitions, of Aqueous Atmospheric Particles, *Chem. Rev.*, 2000, **100**, 3403–3454.
14 A. P. Ault and J. L. Axson, Atmospheric Aerosol Chemistry: Spectroscopic and Microscopic Advances, *Anal. Chem.*, 2017, **89**, 430–452.
15 I. N. Tang and H. R. Munkelwitz, Composition and temperature dependence of the deliquescence properties of hygroscopic aerosols, *Atmos. Environ., Part A*, 1993, **27**, 467–473.
16 D. Gupta, H. Kim, G. Park, X. Li, H.-J. Eom and C.-U. Ro, Hygroscopic properties of NaCl and $NaNO_3$ mixture particles as reacted inorganic sea-salt aerosol surrogates, *Atmos. Chem. Phys.*, 2015, **15**, 3379–3393.
17 M. J. Rood, T. V. Larson, D. S. Covert and N. C. Ahlquist, Measurement of laboratory and ambient aerosols with temperature and humidity controlled nephelometry, *Atmos. Environ. 1967*, 1985, **19**, 1181–1190.
18 C. Denjean, P. Formenti, B. Picquet-Varrault, Y. Katrib, E. Pangui, P. Zapf and J. F. Doussin, A new experimental approach to study the hygroscopic and optical properties of aerosols: application to ammonium sulfate particles, *Atmos. Meas. Technol.*, 2014, **7**, 183–197.
19 S. Ishizaka, K. Yamauchi and N. Kitamura, In situ Quantification of Ammonium Sulfate in Single Aerosol Droplets by Means of Laser Trapping and Raman Spectroscopy, *Anal. Sci.*, 2013, **29**, 1223–1226.
20 L. Wu, X. Li and C.-U. Ro, Hygroscopic Behavior of Ammonium Sulfate, Ammonium Nitrate, and their Mixture Particles, *Asian J. Atmos. Environ.*, 2019, **13**, 16.
21 M. Gysel, E. Weingartner and U. Baltensperger, Hygroscopicity of aerosol particles at low temperatures. 2. Theoretical and experimental hygroscopic properties of laboratory generated aerosols, *Environ. Sci. Technol.*, 2002, **36**, 63–68.
22 N. Wang, B. Jing, P. Wang, Z. Wang, J. Li, S. Pang, Y. Zhang and M. Ge, Hygroscopicity and Compositional Evolution of Atmospheric Aerosols Containing Water-Soluble Carboxylic Acid Salts and Ammonium Sulfate: Influence of Ammonium Depletion, *Environ. Sci. Technol.*, 2019, **53**, 6225–6234.
23 S.-S. Ma, W. Yang, C.-M. Zheng, S.-F. Pang and Y.-H. Zhang, Subsecond measurements on aerosols: from hygroscopic growth factors to efflorescence kinetics, *Atmos. Environ.*, 2019, **210**, 177–185.
24 Z. Ge, A. S. Wexler and M. V. Johnston, Deliquescence Behavior of Multicomponent Aerosols, *J. Phys. Chem. A*, 1998, **102**, 173–180.
25 T. Rosenoern, J. C. Schlenker and S. T. Martin, Hygroscopic Growth of Multicomponent Aerosol Particles Influenced by Several Cycles of Relative Humidity, *J. Phys. Chem. A*, 2008, **112**, 2378–2385.
26 S. Ishizaka, F. Guo, X. Tian, S. Seng, Y. A. Tobon and S. Sobanska, In Situ Observation of Efflorescence and Deliquescence Phase Transitions of Single NaCl and $NaNO_3$

Mixture Particles in Air Using a Laser Trapping Technique, *Bull. Chem. Soc. Jpn.*, 2020, **93**, 86–91.

27 B. N. Fong, J. T. Kennon and H. M. Ali, Mole Ratio Dependence of the Mutual Deliquescence Relative Humidity of Aqueous Salts of Atmospheric Importance, *J. Phys. Chem. A*, 2016, **120**, 3596–3601.

28 A. S. Wexler and S. L. Clegg, Atmospheric aerosol models for systems including the ions H^+, NH^{4+}, Na^+, SO_4^{2-}, NO^{3-}, Cl^-, Br^-, and H_2O, *J. Geophys. Res.: Atmos.*, 2002, **107**(D14), DOI: 10.1029/2001JD000451.

29 L. Treuel, S. Pederzani and R. Zellner, Deliquescence behaviour and crystallisation of ternary ammonium sulfate/dicarboxylic acid/water aerosols, *Phys. Chem. Chem. Phys.*, 2009, **11**, 7976–7984.

30 N. Jordanov and R. Zellner, Investigations of the hygroscopic properties of ammonium sulfate and mixed ammonium sulfate and glutaric acid micro droplets by means of optical levitation and Raman spectroscopy, *Phys. Chem. Chem. Phys.*, 2006, **8**, 2759–2764.

31 M. Trunk, J. F. Lübben, J. Popp, B. Schrader and W. Kiefer, Investigation of a phase transition in a single optically levitated microdroplet by Raman–Mie scattering, *Appl. Opt.*, 1997, **36**, 3305–3309.

32 M. C. Yeung, A. K. Y. Lee and C. K. Chan, Phase Transition and Hygroscopic Properties of Internally Mixed Ammonium Sulfate and Adipic Acid (AS-AA) Particles by Optical Microscopic Imaging and Raman Spectroscopy, *Aerosol Sci. Technol.*, 2009, **43**, 387–399.

33 Q. Zhou, S.-F. Pang, Y. Wang, J.-B. Ma and Y.-H. Zhang, Confocal Raman Studies of the Evolution of the Physical State of Mixed Phthalic Acid/Ammonium Sulfate Aerosol Droplets and the Effect of Substrates, *J. Phys. Chem. B*, 2014, **118**, 6198–6205.

34 Y. Shi, M. Ge and W. Wang, Hygroscopicity of internally mixed aerosol particles containing benzoic acid and inorganic salts, *Atmos. Environ.*, 2012, **60**, 9–17.

35 S. Ghorai, B. Wang, A. Tivanski and A. Laskin, Hygroscopic Properties of Internally Mixed Particles Composed of NaCl and Water-Soluble Organic Acids, *Environ. Sci. Technol.*, 2014, **48**, 2234–2241.

36 S. Potukuchi and A. S. Wexler, Identifying solid-aqueous phase transitions in atmospheric aerosols—I. Neutral-acidity solutions, *Atmos. Environ.*, 1995, **29**, 1663–1676.

37 C. K. Chan and Z. Ha, A simple method to derive the water activities of highly supersaturated binary electrolyte solutions from ternary solution data, *J. Geophys. Res.: Atmos.*, 1999, **104**, 30193–30200.

38 M. D. Cohen, R. C. Flagan and J. H. Seinfeld, Studies of concentrated electrolyte solutions using the electrodynamic balance. 2. Water activities for mixed-electrolyte solutions, *J. Phys. Chem.*, 1987, **91**, 4575–4582.

39 Y. A. Tobon, S. Seng, L. A. Picone, Y. B. Bava, L. C. Juncal, M. Moreau, R. M. Romano, J. Barbillat and S. Sobanska, Photochemistry of single particles using acoustic levitation coupled with Raman microspectrometry, *J. Raman Spectrosc.*, 2017, **48**, 1135–1137.

40 S. Seng, A. L. Picone, Y. B. Bava, L. C. Juncal, M. Moreau, R. Ciuraru, C. George, R. M. Romano, S. Sobanska and Y. A. Tobon, Photodegradation of methyl thioglycolate particles as a proxy for organosulphur containing droplets, *Phys. Chem. Chem. Phys.*, 2018, **20**, 19416–19423.

41 C. A. Schneider, W. S. Rasband and K. W. Eliceiri, NIH Image to ImageJ: 25 years of image analysis, *Nat. Methods*, 2012, **9**, 671–675.

42 G. Biskos, A. Malinowski, L. M. Russell, P. R. Buseck and S. T. Martin, Nanosize Effect on the Deliquescence and the Efflorescence of Sodium Chloride Particles, *Aerosol Sci. Technol.*, 2006, **40**, 97–106.

43 X. Wang, H. Lei, R. Berger, Y. Zhang, H. Su and Y. Cheng, Hygroscopic properties of NaCl nanoparticles on the surface: a scanning force microscopy study, *Phys. Chem. Chem. Phys.*, 2020, **22**, 9967–9973.

44 S. L. Clegg, P. Brimblecombe and A. S. Wexler, Thermodynamic Model of the System $H^+ - NH^{4+} - Na^+ - SO_4^{2-} - NO^{3-} - Cl^- - H_2O$ at 298.15 K, *J. Phys. Chem. A*, 1998, **102**, 2155–2171.

45 J. Sun, L. Liu, L. Xu, Y. Wang, Z. Wu, M. Hu, Z. Shi, Y. Li, X. Zhang, J. Chen and W. Li, Key Role of Nitrate in Phase Transitions of Urban Particles: Implications of Important Reactive Surfaces for Secondary Aerosol Formation, *J. Geophys. Res.: Atmos.*, 2018, **123**, 1234–1243.

46 X. Li, D. Gupta, H.-J. Eom, H. Kim and C.-U. Ro, Deliquescence and efflorescence behavior of individual NaCl and KCl mixture aerosol particles, *Atmos. Environ.*, 2014, **82**, 36–43.

47 P. Vargas Jentzsch, V. Ciobotă, P. Rösch and J. Popp, Reactions of Alkaline Minerals in the Atmosphere, *Angew. Chem., Int. Ed.*, 2013, **52**, 1410–1413.

48 P. Vargas Jentzsch, B. Kampe, V. Ciobotă, P. Rösch and J. Popp, Inorganic salts in atmospheric particulate matter: Raman spectroscopy as an analytical tool, *Spectrochim. Acta, Part A*, 2013, **115**, 697–708.

49 Y. Ebisuzaki, Raman spectra of NH_4Cl and NH_4Br: dependence of the librational and the internal modes of the NH^{4+} ion on volume and on nitrogen–halogen distance, *J. Chem. Phys.*, 1974, **61**, 3170–3180.

50 V. Fawcett, D. A. Long and V. N. Sankaranarayanan, A study of the internal frequency region (400–4000 cm^{-1}) of the Raman spectrum of a single crystal of sodium ammonium sulphate dihydrate, $NaNH_4SO_4{\cdot}2H_2O$ over the temperature range 293–87 K, *J. Raman Spectrosc.*, 1975, **3**, 217–228.

51 V. Ananthanarayanan, Raman spectra of crystalline double sulphates Part II. Ammonium double sulphates, *Z. Für Phys*, 1962, **166**, 318–327.

52 B.-K. Choi, H. J. Labbé and D. J. Lockwood, Raman spectrum of Na_2SO_4 (phase III), *Solid State Commun.*, 1990, **74**, 109–113.

53 B. Xu and G. Schweiger, *in situ* Raman observation of phase transformation of Na_2SO_4 during the hydration/dehydration cycles on single levitated microparticle, *J. Aerosol Sci.*, 1999, **30**, S379–S380.

54 S. Montero, Raman intensities in Na,SO(v) single crystal, *Spectrochimica Acta Part A: Molecular Spectroscopy*, 1976, **32A**, 843–849.

55 A. Hamilton and R. I. Menzies, Raman spectra of mirabilite, $Na_2SO_4{\cdot}10H_2O$ and the rediscovered metastable heptahydrate, $Na_2SO_4{\cdot}7H_2O$, *J. Raman Spectrosc.*, 2010, **41**, 1014–1020.